# Generation and analysis of the proteasome activator PA28-deficient mice

プロテアソーム活性化因子 PA28 ノックアウトマウスの作製と解析

Shigeo Murata

# Generation and analysis of the proteasome activator PA28-deficient mice

(プロテアソーム活性化因子 PA28 ノックアウトマウスの作製と解析)

**Shigeo Murata**

**(村田　茂穂)**

**Contents**

Abstract

The proteasome activator PA28 binds to both ends of the central catalytic machine, known as the 20S proteasome, in opposite orientations to form the enzymatically active proteasome. The PA28 family is composed of three members designated α, β, and γ; PA28α and PA28β form the heteropolymer mainly located in the cytoplasm, while PA28γ forms a homopolymer that predominantly occurs in the nucleus. Available evidence indicates that the heteropolymer of PA28α and PA28β is involved in the processing of intracellular antigens, but the function of PA28γ remains elusive. To investigate the role of PA28γ *in vivo*, mice deficient in the PA28γ gene (Psme3) was generated. The PA28γ-deficient mice were born without appreciable abnormalities in all tissues examined, but their growth after birth was retarded compared with that of PA28γ$^{+/-}$ or PA28γ$^{+/+}$ mice. The effects of the PA28γ deficiency were also investigated using cultured embryonic fibroblasts; cells lacking PA28γ were larger and displayed a lower saturation density than their wild-type counterparts. Neither the expression of PA28α/β nor the subcellular localization of PA28α was affected in PA28γ$^{-/-}$ cells. These results indicate that PA28γ functions as a regulator of cell proliferation and body growth in mice and suggest that neither PA28α nor PA28β compensates for the PA28γ deficiency.

Next, to study the role of PA28α and PA28β *in vivo*, I generated mice deficient for PA28α (Psme1) and PA28β (Psme2) genes simultaneously. Unexpectedly, these mice were embryonic lethal at E9.5-10.5 without specific organ impairments. Northern blot analysis revealed high expression of PA28α and PA28β genes at E7, strongly suggesting that PA28α/β complex plays an indispensable role in early mouse development other than in immune system.

## Introduction

The proteasome with an apparent sedimentation coefficient of 20S is a protein-killing machinery equipped with a variety of catalytic centers that presumably contribute to the hydrolysis of multiple peptide bonds in single polypeptide substrates by a coordinated mechanism (see ref. 1 and references therein). The 20S proteasome is a barrel-like particle with a molecular mass of ~750 kDa, appearing as a stack of four rings made up of two outer α-rings and two inner β-rings (Fig. 1). Tertiary structural analysis indicates that the center of the α-ring is almost closed, thus preventing penetration of substrates into the interior of the β-ring on which the proteolytically active sites are located (2). Presumably because of this structural feature, the 20S proteasome exists as a latent form in cells. The latent proteasome is activated fully by a recently identified endogenous protein, named the proteasome activator PA28 (also known as the 11S regulator) (3, 4). PA28 differs from another well-known proteasome regulator designated PA700. The latter is made up of multiple subunits of 25-110 kDa and associates with the 20S proteasome to form the 26S proteasome, a eukaryotic ATP-dependent protease complex with a molecular mass of ~2 MDa (reviewed in 5-8). The 26S proteasome is responsible for the degradation of a wide variety of cellular proteins tagged with a poly-ubiquitin chain that functions as a degradation signal. Extensive studies conducted during the past decade have established that the 26S proteasome plays a critical role in various biological processes by regulating the levels of cellular proteins rapidly, timely, and/or irreversibly (9, 10).

The native PA28 is a protein complex with a molecular mass of ~200 kDa that binds directly to both ends of the 20S proteasome to form a football-like structure (5, 11). Binding of PA28 greatly stimulates multiple peptidase activities of the 20S proteasome. However, the football-like proteasome lacks the ability to degrade large protein substrates, suggesting that PA28 may cooperate with the 26S proteasome in a sequential proteolytic pathway (2, 3). Indeed, our recent work indicates the existence of a "hybrid-type"

proteasome (12), with PA28 attached to one end and PA700 to another end of the 20S proteasome. Similar to the 26S proteasome, this type of proteasome appears to function as an ATP-dependent protease (Tanahashi et al., manuscript in preparation). PA28 is composed of two subunits, named PA28α and PA28β, that share ~50% amino acid identity (13). These subunits assemble into a heterohexamer (α3β3) with alternating α and β subunits (14) or a heteroheptamer (α3β4 or a mixture of α3β4 and α4β3) (15). Cloning of PA28α and PA28β cDNAs revealed that the α and β subunits are structurally similar to a nuclear protein, termed Ki antigen, which was initially identified with autoantibodies found in sera of patients with systemic lupus erythematosus (13). Ki antigen associates reversibly with the 20S proteasome, indicating that it is a genuine component of the PA28 protein family (16). Therefore, Ki antigen was renamed PA28γ (16). Intriguingly, PA28γ appears to form a homopolymer, presumably $PA28(\gamma)_6$ or $PA28(\gamma)_7$ (16). Upon stimulation with IFN-γ, the protein levels of both PA28α and PA28β increase markedly in a variety of cells, while that of PA28γ remains unchanged or is slightly decreased (reviewed in 17, 18). Furthermore, PA28α and PA28β are located primarily in the cytoplasm, whereas PA28γ occurs in the nucleus without appreciable localization in the cytoplasm (19, 20). Thus, the two forms of the PA28 complex differ in terms of the responsiveness to IFN-γ and subcellular localization.

Proteasomes are the central enzymes responsible for the generation of major histocompatibility complex (MHC) class I ligands (reviewed in 17, 18, 21). Recently, Groettrup et al. (22) found that, together with the MHC-encoded LMP subunits, the IFN-γ-inducible form of PA28 enhances the generation of class I binding peptide by altering the cleavage pattern of the proteasome. More recently, this form of PA28 was found to enhance the induction of virus-specific killer T cells *in vivo* (23) and to favor production of dominant class I ligands *in vitro* (24, 25). These findings suggest that the IFN-γ-inducible PA28 plays an important role in the generation of MHC class I ligands (17). In contrast, no information is available concerning the biological or biochemical function of

the PA28γ homopolymer.

First, to gain insights into the biological function of the PA28γ, mice lacking the PA28γ gene were created. Second, to assess the precise role of the PA28α/β, mice that lack both the PA28α and PA28β genes simultaneously were generated. PA28γ was not essential in mouse development, but its absence resulted in retardation of cell proliferation and body growth. On the contrary, the PA28α and/or PA28β were essential genes, revealing that PA28α/β plays an indispensable role in mouse embryonic development other than in immune system.

## Part I: Growth retardation in mice lacking the proteasome activator PA28γ

### EXPERIMENTAL PROCEDURES

*Construction of the PA28γ Targeting Vector* — A 12-kb *Not*I fragment containing the entire coding region of the PA28γ gene was obtained from a 129/SvJ mouse genomic library (Stratagene) as previously reported (26, 27). The targeting vector consisted of the 6.2-kb genomic DNA containing the 1.2-kb neomycin resistance gene derived from pMC1neopoly(A) (Fig. 2*A*). A 1.1-kb diphtheria toxin gene derived from pMC1DT-3 was attached to the 5' end of the PA28γ-neomycin construct.

*Production of PA28γ Null Mice* — The targeting vector was linearized with *Sal*I and transfected by electroporation into TT2 embryonic stem (ES) cells (courtesy of Dr. S. Aizawa, Kumamoto University). ES cells were selected in 200 μg/ml G418 (GIBCO). Colonies of ES cells with homologous recombination events were identified by polymerase chain reaction (PCR) amplification of a 2.4-kb fragment using the primer pair derived from the 5' upstream region of the PA28γ gene (5'-CACTGCCTAATTGTTGAAAGAGGAGATGCTGTC-3') and from the neomycin gene (5'-GTCTTTTTATTGCCGATCCCCTCAGAAGAACTC-3'). To verify the results of PCR screening, genomic DNAs prepared from the PCR-positive ES clones were digested with *Eco*RI and *Bam*HI, transferred to a nylon membrane (Amersham), and then hybridized with the probe specific for the 5' upstream region of the PA28γ genes (Fig. 2*A*). Expected fragment sizes for wild-type and mutant PA28γ genes were 5.0 kb and 2.0 kb, respectively (Fig. 2*B*).

ES cells heterozygous for the targeted mutation were microinjected into 8 cell-stage ICR mouse embryos, then transplanted into uteri of pseudopregnant BDF1 mice. Chimeric males were crossed to C57BL/6J females. Germline transmission was identified by Southern blot analysis. Progeny containing the mutant PA28γ allele were intercrossed

to obtain PA28γ-deficient mice. Southern blot, Northern blot, and Western blot analyses confirmed disruption of the gene.

*Northern Blot Analysis* — Total RNA was isolated from newborn mice using TRIZOL (GIBCO). Ten μg of total RNA was electrophoresed on a 1% agarose gel and transferred to a nylon membrane. Full-length mouse PA28γ cDNA (26) was labeled with $^{32}P$ using random primers and used as a probe to detect PA28γ mRNAs.

*Western Blot Analysis* — Newborn mice (Fig. 2*D*) or mouse embryonic fibroblasts (MEFs) (Fig6, Fig. 7*A*) were homogenized and solubilized in 1% sodium dodecyl sulfate (SDS) in TE buffer (10 mM Tris-HCl (pH 7.5), 1 mM EDTA). An equal amount of proteins was subjected to SDS-polyacrylamide gel electrophoresis (SDS-PAGE) on a 12.5% gel, transferred onto polyvinylidene difluoride membranes (Millipore), and probed with an anti-PA28α, -PA28β, -PA28γ, or p27 antibody. The antibodies for PA28β and PA28γ were described previously (16). The anti-PA28α antibody raised by immunizing rabbits with full-length recombinant PA28α was a generous gift from Dr. Y. Minami (Oita Medical University). The anti-p27 was purchased from SantaCruz.

*Preparation of MEFs and Cell Culture* — MEFs were obtained from day-13.5 embryos. Cells were cultured at 37°C (5% $CO_2$) in Dulbecco's modified Eagle's medium (DMEM) containing 10% fetal bovine serum (FBS) supplemented with penicillin, streptomycin, L-glutamate, sodium pyruvate, and non-essential amino acids. For G1 synchronization by serum starvation, asynchronous cultures at confluence were placed in DMEM containing 0.1% FBS for 72 h.

*MEF Proliferation Assay* — $4 \times 10^5$ cells of each line were plated in DMEM with 10% FBS in a series of 6-cm culture dishes. Cells were counted daily with a hemocytometer.

*Flow Cytometric Analysis* — For cell size measurement, MEFs were trypsinized, washed with ice-cold PBS, and their forward scatter was measured by FACScan (Becton Dickinson) as soon as possible. For cell cycle analysis, MEFs at logarithmic growth were

pulse-labeled with 10 μM BrdU (Sigma) for 30 min, trypsinized, and fixed in 70% ethanol. For continuous labeling, G1 synchronized cells were trypsinized, replated at a density of 1.5 x $10^6$ cells per 10-cm dish in DMEM with 10% FBS containing 65 μM BrdU, trypsinized after 3, 6, 9, 12, 24 h, and fixed in 70% ethanol. Fixed cells were kept at -20°C until analysis. Cells were treated with 2N HCl to denature the DNA, followed by neutralization by sodium borate. Cells were then incubated with fluorescein isothiocyanate (FITC)-conjugated anti-BrdU antibodies (Pharmingen) and counterstained with propidium iodide containing RNase (20 μg/ml). The stained cells were analyzed on FACScan. Cell debris and fixation artifacts were gated out, and G1, S, and G2/M populations were quantitated using CellQuest software (Becton Dickinson). In each experiment, a similar number of events was analyzed.

For analysis of surface expressions of immunological markers, splenocytes or thymocytes were dispersed into single cells, stained with anti-H2-kb-FITC, anti-CD4-PE, anti-CD8-FITC, anti-CD3-PE, or anti-B220-FITC (Pharmingen), and analyzed on FA Scan.

*Immunocytochemistry* — PA28$\gamma^{+/+}$ and PA28$\gamma^{-/-}$ MEFs were cultured on a slide glass, fixed with 4% paraformaldehyde/PBS, quenched with 50 mM $NH_4Cl$, then permealized with 0.2% Triton X-100/PBS for 30 min at room temperature, and blocked with Blockace (Yukijirushi) overnight at 4°C. Cells were then incubated with a primary antibody solution containing 0.1% Tween-20 for 1h, washed in Triton X-100/PBS, and incubated with a secondary FITC-conjugated anti-rabbit antibody. As a control, nonimmune rabbit sera were used. Cells were embedded in SlowFade (Molecular Probes) mounting medium.

## RESULTS

*Targeted disruption of the PA28γ gene creates a null mutation* — The targeting construct was designed to delete the genomic fragment extending from exon 2 to exon 8

of the PA28γ gene (Fig. 2*A*). PCR screening of 600 colonies resistant to G418 revealed that three ES cell clones underwent homologous recombination. Southern blot analysis with the probe external to the targeting construct confirmed the expected recombination events. Microinjection of PA28γ$^{+/-}$ ES cells into 8 cell-stage ICR embryos produced multiple chimeric males, and germline transmission was demonstrated for chimeras derived from one ES clone. Intercross of the PA28γ$^{+/-}$ mice produced offspring at predicted Mendelian ratios (Table I), suggesting that the PA28γ deficiency did not result in mortality during embryogenesis or fetal development. Southern blot analysis of DNAs extracted from the PA28γ$^{+/-}$ and PA28γ$^{-/-}$ mice confirmed the disruption of the PA28γ gene (Fig. 2*B*). Inactivation of the PA28γ gene was also confirmed by Northern and Western blot analyses (Fig. 2, *C* and *D*). The expression levels in PA28γ$^{+/-}$ heterozygotes were nearly one half of those in PA28γ$^{+/+}$ homozygotes.

*Lack of PA28γ results in small body size* — Following weaning, the PA28γ$^{-/-}$ mice weighed less than sex-matched littermate controls. Representative growth curves in two pairs of such siblings are shown in Fig. 3*A*. A cohort of 177 consecutive intercross breeding was observed up to 12 months of age. During this period, PA28γ-deficient mice were fully viable and fertile.

Analysis of the progeny from intercross breeding showed that, at 24 weeks of age, the mean body weight of PA28γ$^{-/-}$ mice was significantly smaller than that of PA28γ$^{+/+}$ mice in both sexes ($p < 0.01$, see Fig. 3*B* and Table I). The mean body weight was intermediate in PA28γ$^{+/-}$ mice. To examine whether visceral organ size is proportional to the body weight, we measured the wet weight of the heart, liver, spleen, thymus, kidney, and brain. The ratio of organ to body weight was consistently smaller in PA28γ$^{-/-}$ mice than in wild-type mice (data not shown).

*Growth properties of PA28γ -/- MEFs in vitro* — MEFs were prepared from PA28γ$^{+/+}$

and PA28γ$^{-/-}$ embryos 13.5 days postcoitum (dpc), and their growth properties were examined *in vitro*. At passage 4, PA28γ$^{-/-}$ MEFs showed a significantly slower growth rate and a lower saturation density than their wild-type counterparts (Fig. 4*A*). Single MEF size was measured using flow cytometry as forward scatter intensity. PA28γ$^{-/-}$ MEFs were slightly larger than wild-type ones (Fig. 4*B*), consistent with the observation that they showed lower saturation densities.

*Entry into the S phase is impeded in PA28γ$^{-/-}$ MEFs* — To investigate the cause of growth retardation, proliferating MEFs at the logarithmic phase were pulse-labeled with BrdU and analyzed by flow cytometry. As indicated in Fig. 5*A*, PA28γ$^{-/-}$ cells showed an increase in the number of G1 phase cells and a decrease in the number of S phase cells relative to wild-type cells. To confirm this observation, MEFs synchronized at the G1 phase were continuously labeled with BrdU. The percentage of cells that entered the S phase was significantly smaller in PA28γ$^{-/-}$ cells than in wild-type cells (Fig. 5*B*). These results indicate that entry into the S phase is slightly impeded in PA28γ$^{-/-}$ MEFs.

*Degradation rate of p27$^{kip1}$ was not decreased in PA28γ$^{-/-}$ MEFs* —p27$^{kip1}$ is one of the important CDK inhibitors that prevent cells from entering S phase. The expression level of its message is almost indifferent through the cell cycle, and its protein level is regulated by degradation by proteasome. As the phenotypes of PA28γ$^{-/-}$ MEFs resembled those of p27$^{kip1}$ overexpressing cells in the respects of cell enlargement and impediment of G1/S transition, I expected the slower degradation of p27 in PA28γ$^{-/-}$ MEFs. G1 synchronized MEFs were replated in medium containing 10% FCS, and the p27 protein levels were chased for the indicated time (Fig.6). Western blot analysis revealed no significant differences of the protein level and the degradation rate of p27 protein between wild-type and PA28γ$^{-/-}$ cells.

*Expression of PA28α and PA28β in PA28γ-deficient cells* — We next examined whether the absence of PA28γ influences the expression of PA28α or PA28β. Western blot analysis using MEF extracts showed that the levels of neither PA28α nor PA28β are affected by the deficiency of PA28γ (Fig. 7*A*). Under normal conditions, PA28α and PA28β are co-localized predominantly in the cytoplasm, whereas PA28γ occurs mainly in the nucleus (19, 20). However, PA28α has two possible nuclear localization signals (27). Therefore, it was of interest to examine whether the PA28α/β complex can enter the nucleus in the absence of PA28γ and compensate for the deficiency of PA28γ. As shown in Fig. 7*B*, immunocytochemical analysis of PA28γ$^{+/+}$ MEFs indicated that PA28γ is located predominantly in the nuclei excluding the nucleoli (right upper panel), as reported before (19, 20). No significant staining was observed in PA28γ$^{-/-}$ cells (right lower panel). On the other hand, the subcellular distribution of PA28α was essentially the same between PA28γ$^{-/-}$ and PA28γ$^{+/+}$ MEFs (left upper and lower panels). Thus, the PA28α/β heteropolymer is unlikely to take over the function of PA28γ in PA28γ-deficient cells.

*Immunological aspects of PA28γ$^{-/-}$ mice*—As PA28α/β complex is regarded as enhancer of MHC class I ligand production by proteasomes, the possibility that PA28γ also participates in antigen processing was examined. Expression levels of surface MHC class I (Fig. 8A), cell numbers in spleen or thymus (Fig. 8B), CD4/CD8 ration in thymus or spleen (Fig. 8 C, D), T cell/ B cell ration in spleen were analyzed using flow cytometry, but no significant differences were not found between wild-type and homozygous mice.

## DISCUSSION

In this report, I generated PA28γ-deficient mice by gene targeting (Fig. 2) and found that PA28γ affects body size, cell growth, and cell proliferation (Figs. 2 and 3). Flow cytometric analysis of MEFs (Fig. 5) revealed that the proportion of cells that entered the S phase was significantly lower in PA28γ$^{-/-}$ cells than in wild-type cells. The PA28γ

homopolymer can associate with the 20S proteasome (16) and stimulate the latent proteasome activity strongly (28). Thus, the phenotype of PA28γ-deficient mice raises the possibility that PA28γ might be involved in the degradation of nuclear proteins regulating cell-cycle progression. For example, loss of PA28γ may delay the degradation of CDK inhibitors such as $p21^{cip1}$ and $p27^{kip1}$, the degradation of which is required for G1 to S transition in the cell cycle (29). We, therefore, examined the protein levels of p27 in $PA28\gamma^{-/-}$ and $PA28\gamma^{+/+}$ MEFs by Western blot analysis, but could not find any obvious difference (Fig. 6).

A series of recent studies have established that the PA28α/β complex is involved in the generation of MHC class I ligands (reviewed in 17, 18, 22). We, therefore, investigated whether PA28γ-deficient mice show any abnormalities in their immune system. The cellularity and size of the spleen and thymus did not show any obvious difference between $PA28\gamma^{-/-}$ and wild-type mice (Fig. 8). Furthermore, disruption of the PA28γ gene did not alter the CD4/CD8 ratios in thymocytes and splenocytes, the T/B cell ratio in peripheral lymphocytes, or the expression level of cell surface MHC class I molecules (Fig. 8). These results indicate that PA28γ is unlikely to play a pivotal role in the MHC class I antigen processing/presentation system. This is consistent with the observation that PA28γ has been found in invertebrates that do not have the adaptive immune system (26). However, the present study does not rule out the possibility that PA28γ plays a specialized role in antigen presentation such as the processing of antigens in the nucleus.

Since PA28γ localizes almost exclusively in the nucleus and is highly conserved between vertebrates and invertebrates, it was supposed that PA28γ might have an essential role in maintaining cellular activities. Contrary to this initial expectation, PA28γ turned out to be dispensable. Subcellular localization of PA28α, and hence, that of the PA28α/β complex did not change significantly between PA28γ-deficient and wild-type cells (Fig. 6). Thus, it appears unlike that dispensability of PA28γ ensues from the

compensation provided by the PA28α/β complex. A better understanding of the biological functions of the PA28 family proteins might be gained by creating mutant mice lacking all three members of this family. Such work is now in progress.

## Part II: Loss of the proteasome activator PA28α and PA28β causes lethality before 10.5 days of gestation in mice

### EXPERIMENTAL PROCEDURES

*Construction of the PA28α and PA28β Targeting Vector* — A 15-kb *Not*I fragment (λA6) containing the entire coding region of the PA28α gene and a 23-kb *Not*I fragment containing the entire coding region of the PA28β gene (λB2) were obtained from a 129/SvJ mouse genomic library (Stratagene) as previously reported (26, 27). The targeting vector consisted of the 7.5-kb genomic DNA upstream of the PA28β gene, the 1.2-kb neomycin resistance gene derived from pMC1neopoly(A), the 6.5-kb genomic DNA that lies between the PA28α gene and the PA28β gene, and the 2.2-kb genomic DNA upstream of the PA28α gene (Fig. 7A). A 1.1-kb diphtheria toxin gene (DT-A) derived from pMC1DT-3 was attached to the 5' end of the above 2.2-kb fragment for negative selection.

*Production of PA28α/β Null Mice* — The targeting vector was linearized with *NotI* and transfected by electroporation into TT2 embryonic stem (ES) cells. ES cells were selected in 200 μg/ml G418 (GIBCO). Colonies of ES cells with homologous recombination events were identified by polymerase chain reaction (PCR) amplification of a 4.2-kb fragment of wild-type allele and a 2.2-kb fragment of mutated allele using the primer pair derived from the 5' upstream region of the PA28α gene (5'-TTTCCTGTACGTGACTTCCATCCTGTTG-3', a-S) and from the genomic DNA that lies between the two genes (5'-GGTCCACATACAATAAAGACATGGGCTG-3', a-AS). To verify the results of PCR screening, genomic DNAs prepared from the PCR-positive ES clones were digested with *BamHI* to detect homologous recombination events for PA28α gene and *ScaI* and *BssHII* to detect homologous recombination events for PA28β gene, transferred to a nylon membrane (Amersham), and then hybridized with the probe specific for the 5' upstream region of the PA28α genes and PA28β genes, respectively

(Fig. 7A). Expected fragment sizes for wild-type and mutant PA28α genes were 2.3-kb and 4.0-kb, respectively. Expected fragment sizes for wild-type and mutant PA28β genes were 13.0-kb and 8.0-kb, respectively.

ES cells heterozygous for the targeted mutation were microinjected into 8 cell-stage ICR mouse embryos, then transplanted into uteri of pseudopregnant BDF1 mice. Chimeric males were crossed to C57BL/6J females. Germline transmission was identified by Southern blot analysis. Progeny containing the mutant PA28α/β allele were intercrossed to obtain PA28α/β-deficient mice.

*Genotyping of mice embryos* — Mice embryos were obtained from heterozygous female mice mated with male heterozygous mice. Embryonic yolk sacs were incubated in buffers containing proteinase K and pronase E (50mM Tris-HCl (pH 8.0), 100mM NaCl, 20mM EDTA, 1% SDS, 150μg/ml proteinase K, 1mg/ml pronase E) at 50℃ for three hours and used for PCR to determine the genotypes of the embryos. For the genotyping of PA28α gene, the primers a-S, a-AS, and the primer derived from the deleted region of the PA28α gene (5'-GATTGTGGTCCTCCTGCAACGCCTAAA-3', a-del) were used (Fig. 7A), and the resulting fragment sizes are 1.2-kb and 4.2-kb for wild-type allele and 2.2-kb for mutated allele. For the genotyping of PA28β gene, the primer derived from the deleted region of the PA28β gene (5'-CTTCTGGCCTTGCTCGCTTTGGTTAA-3', b-S), the primer derived from the 3' downstream genomic DNA of PA28β gene (5'-ATTCCTCCAGTCAACCCTCTCCCAC-3', b-AS), and the primer derived from neomycin-resistant gene (5'-GTTTGCTCGACATTGGGTGGAAACATT-3', b-Neo) were used (Fig. 7A), and the resulting fragment sizes are 1.9-kb for wild-type allele and 0.35-kb for mutated allele.

*Northern Blot Analysis* — A filter which was blotted 2μg of polyA RNA per lane from four mouse embryos of different developmental stages were purchased from Clontech (Mouse Embryo MTN Blot). Full-length mouse PA28α, PA28β, and PA28γ cDNA (26) were labeled with $^{32}P$ using random primers and used as a probe to detect PA28α and

PA28β mRNAs. As a control, human β-actin cDNA was used.

## RESULTS

*Simultaneous targeting of the PA28α and PA28β genes* — The targeting construct was designed to delete the genomic fragments extending from exon 2 to exon 10 of the PA28α gene and from exon 1 to exon 10 of the PA28β gene (Fig. 7A). Genomic region that lies between the two genes was completely preserved. PCR screening of 120 colonies resistant to G418 revealed that two ES cell clones underwent homologous recombination. Southern blot analysis with the probe external to the targeting construct confirmed the expected recombination events (Fig. 7B). Microinjection of PA28α/β$^{+/-}$ ES cells into 8 cell-stage ICR embryos produced multiple chimeric males, and germline transmission was demonstrated for chimeras derived from one ES clone.

*Deficiency of PA28α and PA28β results in embryonic lethality* — The PA28α/β heterozygous mice were intercrossed, and pups were born at the 1:2 ratio of wild type to heterozygous, but no homozygous mutant pups were obtained from any litter (Table2). To determine the time of embryonic death and to characterize the morphological phenotype of the mutant embryos, different stages of gestation were analyzed for the presence of PA28α/β$^{-/-}$ offsprings. The genotype of the yolk sacs was determined by PCR (Fig. 7C). During early stages of development, from embryonic day (E) 8.5 to E9.5, PA28α/β$^{-/-}$ embryos could be detected with almost the expected Mendelian frequency and were indistinguishable from their littermates by external appearance. At E 10.5, no viable PA28α/β$^{-/-}$ embryos were found. Mutant fetuses showed arrested and swollen heart, blood-filled vessels in the embryonic body, and pale yolk sacs, but almost the same size as their littermates (Fig. 8). Embryonic structures bearing a PA28α/β$^{-/-}$ genotype could be recovered up to E11.5. However mutant embryos from this stage showed the most obvious deterioration, and an increased number of resorptions was observed. Histological

examination of E9.5 and E10.5 embryonic bodies and placentas were performed. Microscopic analysis showed that mutant embryos had apparently normal livers, hearts, dorsal aortas, branchial arches, vitelline vasculatures, hematopoietic cells, livers, and placentas (data not shown), whose abnormalities are often the causes of embryonic lethality around E7.5-12.5.

*PA28α and PA28β are strongly expressed in early development* — The early embryonic lethal phenotype of PA28α/β-deficient embryos suggested that PA28α/β complex has an indispensable function during fetal development other than immunological function. To understand its role in development, analysis of expression pattern of the PA28α and PA28β genes during stages of mouse development between E7 and E17 was performed. Northern blot analysis revealed extremely high expression levels of PA28α and PA28β messages at E7, drastic decrease at E11, and gradual increase toward E17, whereas the expression levels of PA28γ messages were almost constant (Fig. 9). This data suggests the existence of critical roles of PA28α/β complex in early fetal development.

## DISCUSSION

The results reported here provide the first genetic evidence that PA28α/β complex plays an indispensable role in development. Until now, various studies have shown the evidences that PA28α/β complex has an important role in immune system, especially cytotoxic T cell response for viruses (17,18). Quite recently, Y.Yang and his colleagues published the results of PA28β-deficient mice (35). They focused the analyses on immunological function of PA28. In PA28β-deficient mice, PA28α was also decreased and assembly of immunoproteasome was greatly impaired. Lymphocytes from PA28β-deficient mice couldn't present viral antigens as well as those from wild-type mice. These data confirmed that PA28α/β complex plays very important roles in antigen processing

and presentation. In their report, PA28β-deficient mice were born healthy. However, the fact that PA28α/β-deficient mice die *in utero* at E9.5-10.5 strongly suggests its pivotal role in fundamental biological functions other than in immunity. The high expressions of mRNA for both PA28α and PA28β at E7 and their sudden decrease at E11 may be related to embryonic death during E9.5-10.5. There have been some studies that indicate the existence of non-immunological function of PA28. Although PA28α/β can be up-regulated by IFN-γ, the degree of their increase is much smaller than those of TAP1, TAP2, LMP2, LMP7, and MHC class I heavy chains, which are the main players of MHC class I antigen processing and presentation (Murata, unpublished data), and PA28α and PA28β are constitutively expressed considerable amount ubiquitously (16). Many tumor cells alter the expression of proteins involved in antigen processing and presentation, allowing them to avoid recognition and elimination by cytotoxic T cells. Johnsen et al (30) examined the expression levels of genes concerning MHC class I presenting pathway including PA28α and PA28β in various tumor cell lines. In some cases, complete deficiencies were observed in the expression of the TAP1, TAP2, LMP2, LMP7, and MECL1. On the contrary, expression levels of PA28α and PA28β were unaltered in all cell lines. This suggests that PA28α/β may influence viability and growth of these cells independent of antigen processing. Moreover, PA28α is found to interact with the protein kinase B-Raf (31), which acts as signal transducing elements downstream of activated cell surface receptors and is involved in the regulation of proliferation, differentiation, and cell survival, although the meaning of this interaction is unsolved.

The cause of lethality in PA28α/β-deficient mice is still unknown. The causes of embryonic death during early organogenesis are limited from the results of various knockout mice. The first type falls into failure of haematopoiesis and cardiovascular development such as knockout mice of vascular endothelial growth factor (VEGF) and their receptors (32). However, our knockout mice didn't show obvious abnormalities in cardiovascular system, and erythrocytes were abundant. So this doesn't seem to be the

case. The second type is failure to establish chorioallantoic placenta such as Mash2 (33) and estrogen-receptor β (ERR-β) (34). These mice died at almost the same embryonic day as PA28α/β-deficient mice, but they showed growth retardation *in utero* before death, and the histological structures of the placenta were abnormal. On the contrary, PA28α/β knockout mice didn't show growth retardation nor abnormal placental histology. Therefore, it is presumed that PA28α/β mice may die for a novel cause. Since chorioallantoic circulation establishes at E9.5-10.5, a novel stress for embryos from maternal body, for example oxygenation, may cause the systemic failure and lead to death. Minami and his colleagues revealed a novel function of PA28 recently (unpublished data). They found that PA28α/β complex fully reactivate heat inactivated luciferase in cooperation with Hsp90, Hsp70, and Hsp40. They also showed that PA28α homopolymer, without PA28β, could play the role. These data showed the existence of chaperone activity of PA28, which does not necessarily require PA28β. Loss of the chaperone activity of PA28 may cause the embryonic lethality of our PA28α/β-deficient mice.

To determine the responsible organs and to investigate the function of viable organs such as lymphocytes, attempts to generate chimeric mice between PA28α/β knockout mice and wild-type or $RAG2^{-/-}$ mice are currently in progress.

**Acknowledgements**

It is a great honor to acknowledge my supervisors, Professor Kazuhiko Yamamoto and Director Keiji Tanaka, who continue to lead me to a more advanced academic sphere and have given me invaluable advice and instruction enabling me to successfully complete all of my academic requirements during my four years of study. I am deeply grateful to my experimental instructor Dr. Tomoki Chiba for his guidance and valuable suggestions in the experiments of this project. I also owe a great debt of gratitude to all of my colleagues in the department of allergy and rheumatology, University of Tokyo, and department of molecular oncology, Tokyo Metropolitan Institute of Medical Science.

## References


1. Coux, O., Tanaka, K., and Goldberg, A. L. (1996) *Annu. Rev. Biochem.* **65**, 801-847.
2. Groll, M., Ditzel, L., Lowe, J., Stock, D., Bochtler, M., Bartunik, H. D., and Huber, R. (1997) *Nature* **386**, 463-471.
3. Ma, C. P., Slaughter, C. A., and DeMartino, G. N. (1992) *J. Biol. Chem.* **267**, 10515-10523.
4. Dubiel, W., Pratt, G., Ferrell, K., and Rechsteiner, M. (1992) *J. Biol. Chem.* **267**, 22369-22377.
5. Baumeister, W., Walz, J., Zühl, F., and Seemüller, E. (1998) *Cell* **92**, 367-380.
6. Rechsteiner, M. (1998) The 26S proteasome. In "Ubiquitin and the Biology of the Cell" (Eds by Peters, J.-M., Harris, J. R. & Finley, D.) pp147-189, Plenum Press, New York.
7. DeMartino, G. N. and Slaughter, C. A. (1999) *J. Biol. Chem.* **274**, 22123-22126.
9. Hershko, A. and Ciechanover, A. (1998) *Annu. Rev. Biochem.* **67**, 425-479.
10. Ciechanover, A. (1998) *EMBO J.* **17**, 7151-7160.
11. Gray, C. W., Slaughter, C. A. and DeMartino, G. N. (1994) *J. Mol. Biol.* **236**, 7-15.
12. Hendil, K. B., Khan, S., and Tanaka, K. (1998) *Biochem. J.* **332**, 749-754.
13. Ahn, J. Y., Tanahashi, N., Akiyama, K., Hisamatsu, H., Noda, C., Tanaka, K., Chung, C. H., Shibmara, N., Willy, P. J., Mott, J. D., Slaughter, C. A., and DeMartino, G. N. (1995) *FEBS Lett.* **366**, 37-42.
14. Song, X., Mott, J. D., von Kampen, J., Pramanik, B., Tanaka, K., Slaughter, C. A., and DeMartino, G. N. (1996) *J. Biol. Chem.* **271**, 26410-26417.
15. Zhang, Z., Krutchinsky, A., Endicott, S., Realini, C., Rechsteiner, M., and Standing, K. G. (1999) *Biochemistry* **38**, 5651-5658.
16. Tanahashi, N., Yokota, K., Ahn, J. Y., Chung, C. H., Fujiwara, T., Takahashi, E., DeMartino, G. N., Slaughter, C. A., Toyonaga, T., Yamamura, K., Shimbara, N., and Tanaka, K. (1997) *Genes to Cells* **2**, 195-211.

17. Tanaka, K., and Kasahara, M. (1998) *Immunol. Rev.* **163**, 161-176.

18. Fruh, K., and Yang, Y. (1999) *Curr. Opin. Immunol.* **11**, 76-81.

19. Soza, A., Knuehl, C., Groettrup, M., Henkliein, P., Tanaka, K., and Kloetzel, P.-M. (1997) *FEBS Lett.* **413**, 27-34.

20. Wojcik, C., Paweletz, N., Tanaka, K., and Wilk, S. (1998) *Eur. J. Cell. Biol.* **77**, 151-160.

21. Rock, K. L. and Goldberg, A. L. (1999) *Annu. Rev. Immmunol.* **17**, 739-779.

22. Groettrup, M., Ruppert, T., Kuehn, L., Seeger, M., Standera, S., Koszinowski, U., and Kloetzel, P.-M. (1995) *J. Biol. Chem.* **270**, 23808-23815.

23. Groettrup, M., Soza, A., Eggers, M., *et al.* (1996) *Nature* **381**, 166-168.

24. Dick, T.P., Ruppert, T., Groettrup, M., Kloetzel, P.M., Kuehn, L., Koszinowski, U. H., Stevanovi'c, S., Schild, H., and Rammensee, H.-G. (1996) *Cell* **86**, 253-262.

25. Shimbara, N., Ogawa, K., Nakajima, H., Yamasaki, N., Hidaka,Y., Niwa. S., Tanahashi, N., and Tanaka. K. (1998) *J. Biol. Chem.* **273**, 23062-23071.

26. Kandil, E., Kohda, K., Ishibashi, T., Tanaka, K., and Kasahara, M. (1997) *Immunogenetics* **46**, 337-344.

27. Kohda, K., Ishibashi, T., Shimbara, N., Tanaka, K., Matsuda, Y., and Kasahara, M. (1998) *J. Immunol.* **160**, 4923-4935.

28. Realini, C., Jensen, C. C., Zhang, Z., Johnsto, S. C., Knowlton, J. R., Hill, C. P., and Rechsteiner, M. (1997) *J. Biol. Chem.* **272**, 25483-25492.

29. Sherr, C. J. and Roberts, J. M. (1999) *Genes & Dev.* **13**, 1501-1512.

30. Johnse, A., France, J., Sy, M., and Harding, C. V. (1998) *Cancer Res.* **58**, 3660-3667.

31. Kalmes, A., Hagemann, C., Weber, C. K., Wixler, L., Shuster, T., and Rapp, U. R. (1998) *Cancer Res.* **58**, 2986-2990.

32. Korpelainen, E. I. And Alitalo, K. (1998) *Curr Opin Cell Biol.* **10**, 159-64.

33. Guillemot, F., Caspary, T., Tilghman, S. M., Copeland, N. G., Gilbert, D. J., Jenkins,

N. A., Anderson, D.J., Joyner, A. L., Rossant, J., and Nagy, A. (1995) *Nature Genetics*. **9**, 235-242.

34. Luo, J., Sladek, R., Bader, J., Matthyssen, A., Rossant, J., and Giguere, V. (1997) *Nature*. **388**, 778-782.

35. Preckel, T., Fung-Leung, WP., Cai ,Z., Vitiello, A., Salter-Cid, L., Winqvist ,O., Wolfe, TG., Von Herrath, M., Angulo ,A., Ghazal, P., Lee, JD., Fourie ,AM., Wu, Y., Pang, J., Ngo, K., Peterson, PA., Fruh, K., Yang, Y. (1999) *Science* **286**, 2162-5 .

**TABLE I**

**Number of offsprings resulting from intercrossing of PA28γ+/- mice and the weight of each genotype at the age of 24 weeks.**

| | | | Body weight |
|---|---|---|---|
| Sex | Genotype | Number | Mean ± S.D.(grams) |
| Male | +/+ | 16 | 32.9 ± 3.8 |
| | +/- | 44 | 31.0 ± 3.1 |
| | -/- | 23 | 29.5 ± 3.2 |
| Female | +/+ | 22 | 23.9 ± 3.4 |
| | +/- | 46 | 23.2 ± 2.8 |
| | -/- | 26 | 21.7 ± 2.9 |

## TABLE II

**Number of offsprings resulting from PA28α/β+/- intercross, survival mutants, and absorbed embryos**

| Stage | genotype | | | Survival -/- | Absorbed |
|---|---|---|---|---|---|
| | +/+ | +/- | -/- | | |
| Neonate | 7 | 14 | 0 | 0 | - |
| E13.5 | 5 | 6 | 0 | 0 | 5 |
| E11.5 | 1 | 1 | 4 | 0 | 1 |
| E10.5 | 13 | 30 | 13 | 0 | 5 |
| E9.5 | 5 | 38 | 18 | 18 | 1 |
| E8.5 | 1 | 6 | 1 | - | 0 |

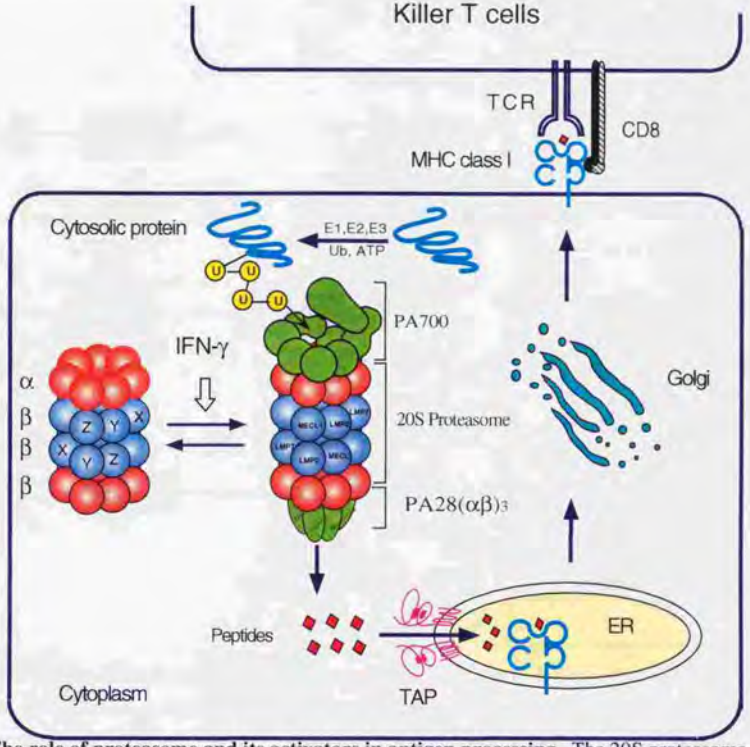


**Fig. 1 The role of proteasome and its activators in antigen processing.** The 20S proteasome is a barrel-like particle composed of four rings made up of two α-rings and two β-rings, and exists as a latent form. Two proteasome activators, PA700 and PA28 activate the latent proteasome. Polyubiquitinated cytosolic proteins are captured and fed into 20S proteasome by PA700 and degraded into peptides in ATP dependent manner. PA28 stimulates the peptidase activity of the 20S proteasome, supplying MHC class I ligands more efficiently in cooperation with LMP7, LMP2, and MECL1, which replaces the constitutive subunits of the 20S proteasome upon IFN-γ stimulation.

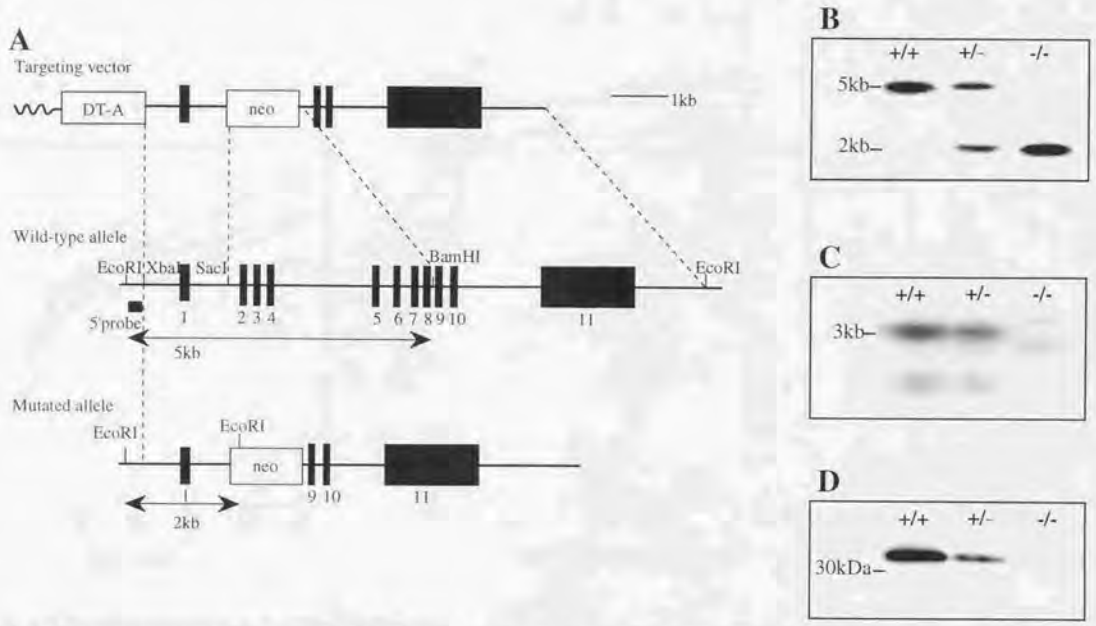


**Fig. 2 Targeted disruption of the mouse PA28γ (*Psme3*) gene.** *A*, The structure of the targeting vector, the restriction map of the mouse PA28γ gene, and the structure of the mutated allele following the homologous recombination. The exons are depicted by closed boxes and are numbered. A single probe to the 5' end of the PA28γ gene (shown as the 5' probe) was used to identify recombinant alleles at 2 kb and wild-type alleles at 5 kb, following *Eco*RI and *Bam*HI digestion of genomic DNA. *B*, Southern blot analysis of DNA from mice obtained by intercross breeding of heterozygous mice. Mice from intercross breeding were genotyped using tail DNA digested with *Eco*RI and *Bam*HI. *C*, Northern blot analysis of total RNA prepared form PA28$\gamma^{+/+}$, PA28$\gamma^{+/-}$, and PA28$\gamma^{-/-}$ mice. Full-length mouse PA28γ cDNA (26) was 32P-labeled using random primers and used as a probe. *D*, Western blot analysis of extracts prepared from PA28$\gamma^{+/+}$, PA28$\gamma^{+/-}$, and PA28$\gamma^{-/-}$ mice. The blot was probed with the anti-PA28γ antibody.

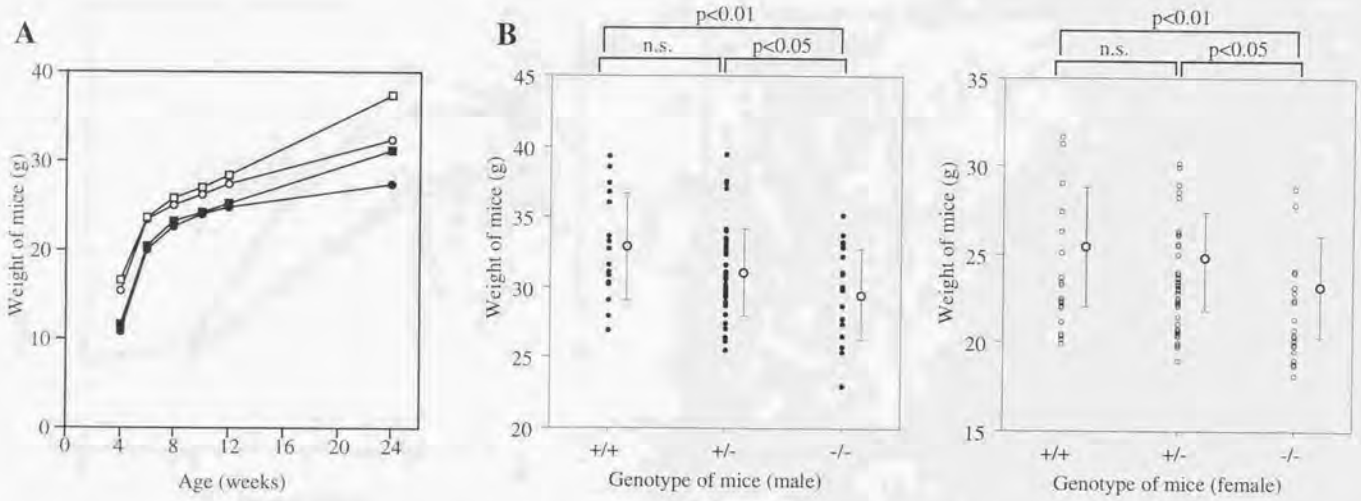


**Fig. 3 Growth retardation in PA28γ-deficient mice.** *A*, Growth curves in two pairs of male littermates. Each pair is represented by a square or circle symbol. Open and filled symbols indicate wild-type and PA28γ-deficient mice. Mice were weighed at indicated intervals and their weight was plotted against age in weeks. *B*, Analysis of body weight in a total of 175 mice obtained by intercross breeding of PA28γ+/- heterozygotes. Body weight in 85 male mice (left) and 90 female mice (right) at 24 weeks of age is shown. There are statistically significant differences between the $PA28\gamma^{-/-}$ and $PA28\gamma^{+/+}$ groups ($p < 0.01$) and between the $PA28\gamma^{-/-}$ and $PA28\gamma^{+/-}$ group ($p < 0.05$) in both male and female cohorts. Statistical analysis was performed by one-way ANOVA and Sheffe's method as Post-Hoc test (male: ANOVA; $F(2,80) = 4.995$, $p = 0.009$, female: ANOVA; $F(2,91) = 3.747$, $p = 0.0273$).

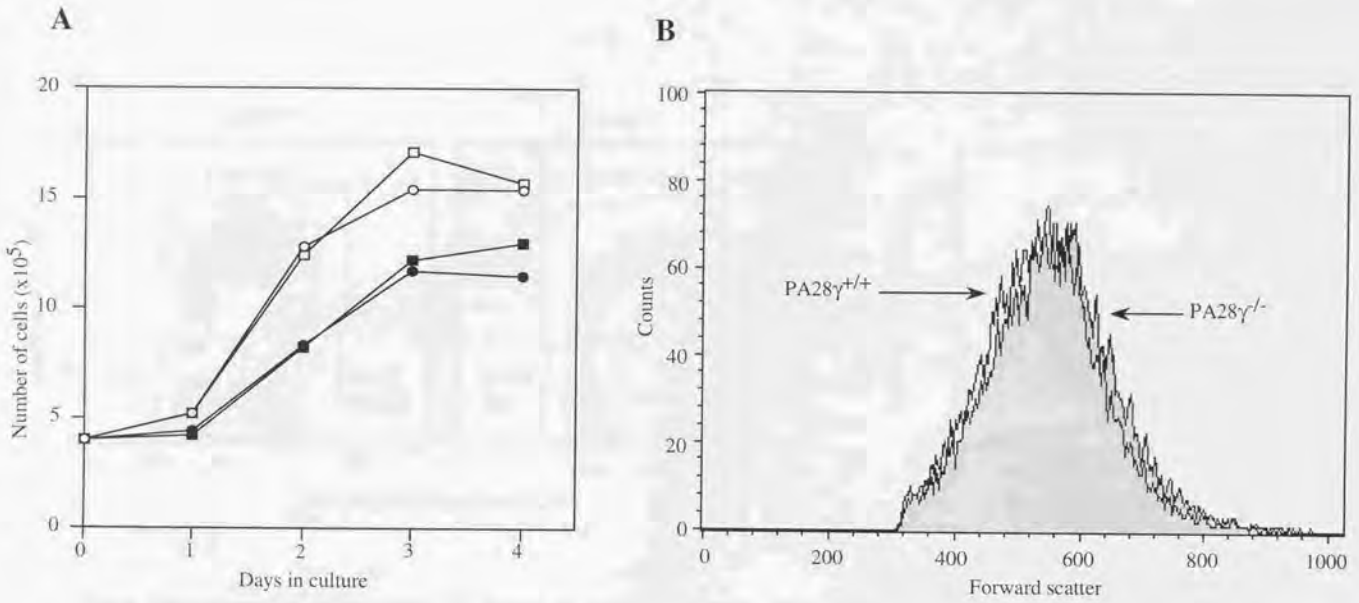


**Fig. 4 Growth properties and single cell size of MEFs.** *A*, Growth kinetics and saturation densities of primary MEFs at passage 4. Cells ($4 \times 10^5$) from wild-type (open symbols) and PA28$\gamma^{-/-}$ (filled symbols) were plated in 60-mm culture dishes and counted daily. Two independent pairs of MEFs (represented by circle and square symbols) were used. *B*, Single cell size of MEF with a wild-type or PA28γ-deficient genotype. MEFs were harvested at the logarithmic growth phase. Forward scatter intensity was measured by flow cytometry. Open and filled histograms indicate wild-type and PA28$\gamma^{-/-}$ MEFs, respectively.

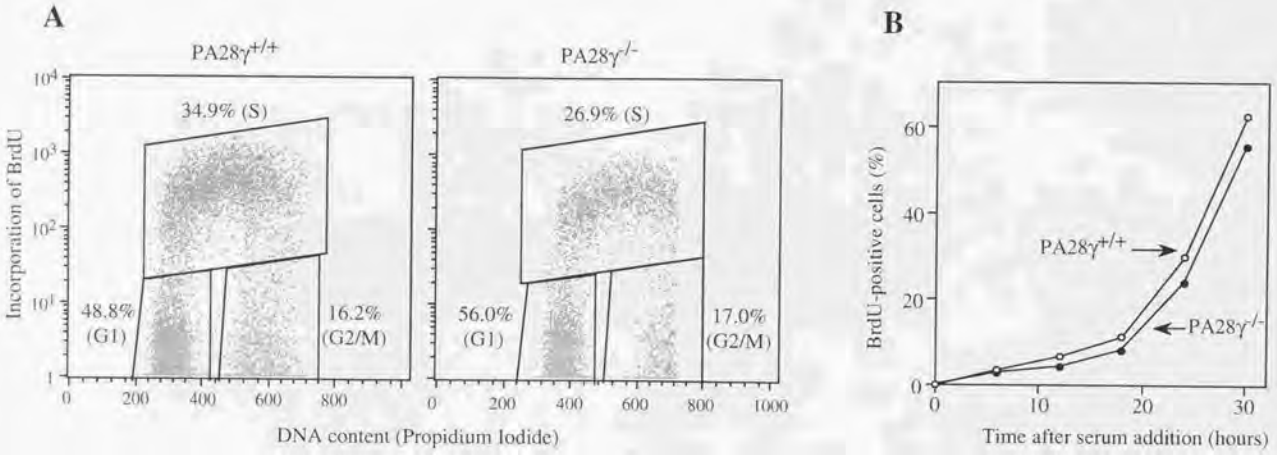


**Fig. 5 Flow cytometric analysis of asynchronous and synchronized MEFs.** *A*, Representative two-color flow cytometric analyses of asynchronous passage-4 MEF cells. MEFs at the logarithmic growth phase were labeled with 10 μM BrdU for 30 min prior to harvest. Cells were stained with propidium iodide for DNA content and with an FITC-conjugated anti-BrdU antibody for measuring replicative DNA synthesis. Gates are indicated by G1 (lower left), S (upper middle), and G2/M (lower right). Left panel, PA28γ+/+ MEF cells; right panel, PA28γ-/- MEF cells. The percentage of cells in each phase of the cell cycle is indicated. Approximately $10^4$ cells were examined in each analysis, and experiments were repeated four times. *B*, MEFs at confluence were cultured for 72 h in serum-starved media, then replated onto 10-cm dishes at a density of 1.5 x $10^6$/dish in complete media containing 65 μM BrdU. Cells were harvested at indicated time intervals and stained as above. Experiments were repeated three times.

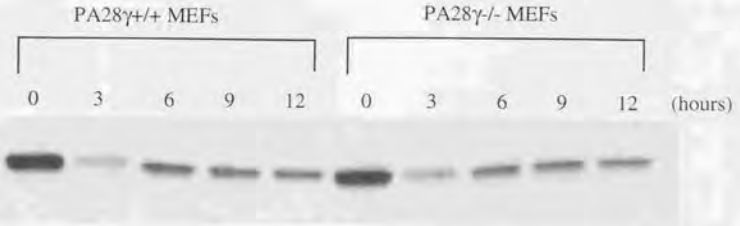


**Fig.6 Degradation rate of $p27^{kip1}$ in synchronized MEFs.** MEFs were synchronized at G1 phase by serum starvation, then replated onto 10cm-dishes at a density of $1.5x10^6$/dish in complete media containing 10% FCS. Cells were lyzed 0, 3, 6, 9, 12 hours after serum addition, and their extracts were analyzed by Western blot using anti-$p27^{kip1}$ antibody.

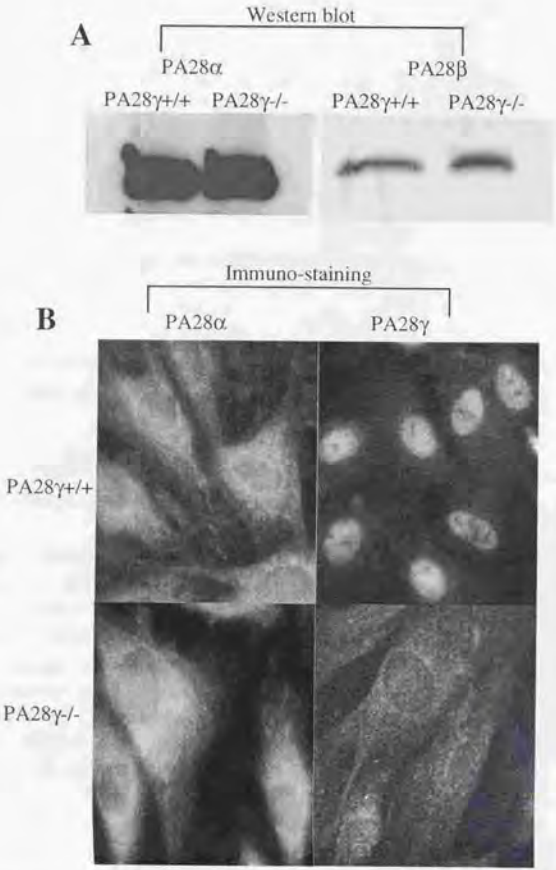


**Fig.7 Expression of PA28α and PA28β in PA28γ-deficient cells.** *A*, Western blot analysis of extracts prepared from wild-type and PA28γ-/- MEFs. The blot was probed with the anti-PA28α or anti-PA28β antibody. *B*, Immunocytochemical staining. MEFs on the slide glass were fixed, permealized, and stained with the first antibody (anti-PA28α or anti-PA28γ), followed by the FITC-conjugated second antibody.

A

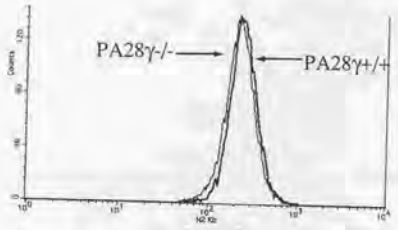


B

| | thymus | spleen |
|---|---|---|
| wild-type | $2.0 \pm 0.3 \times 10^8$ | $7.8 \pm 0.6 \times 10^8$ |
| PA28γ-/- | $1.8 \pm 0.4 \times 10^8$ | $8.0 \pm 0.7 \times 10^8$ |

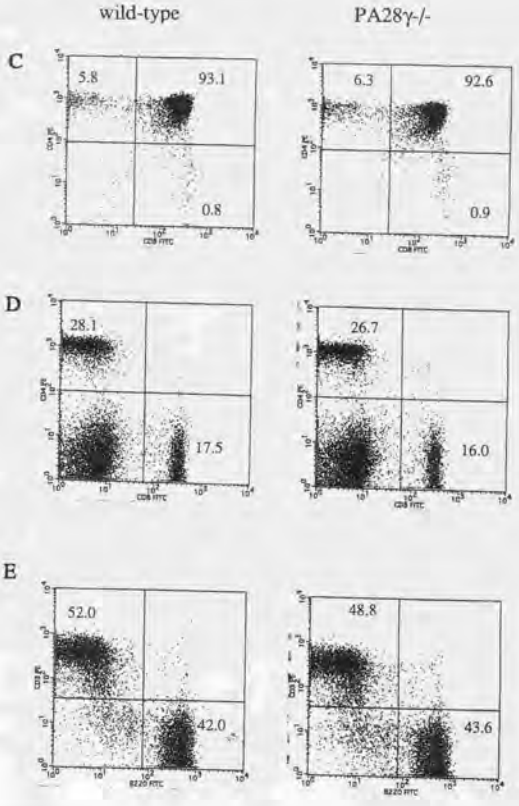


**Fig. 8 Immunological aspects of PA28γ-/- mice.** *A*, Surface MHC class I (H2-Kb) expression of splenocytes from 4-week old male mice were analyzed by FACScan. *B*, Cellularity of spleens and thymus of wild-type and PA28γ-/- mice. Results show means ± S.D. of three mice. *C*, Population of CD4-single positive, CD8-single positive, and CD4/CD8-double positive lymphocytes in thymus of 4-week old male mice. *D*, Population of CD4-positive and CD8-positive lymphocytes in spleens of 4-week old male mice. *E*, Population of CD3-positive and B220-positive lymphocytes in spleens of 4-week old male mice.

# Simultaneous targeting of the mouse PA28α and PA28β genes

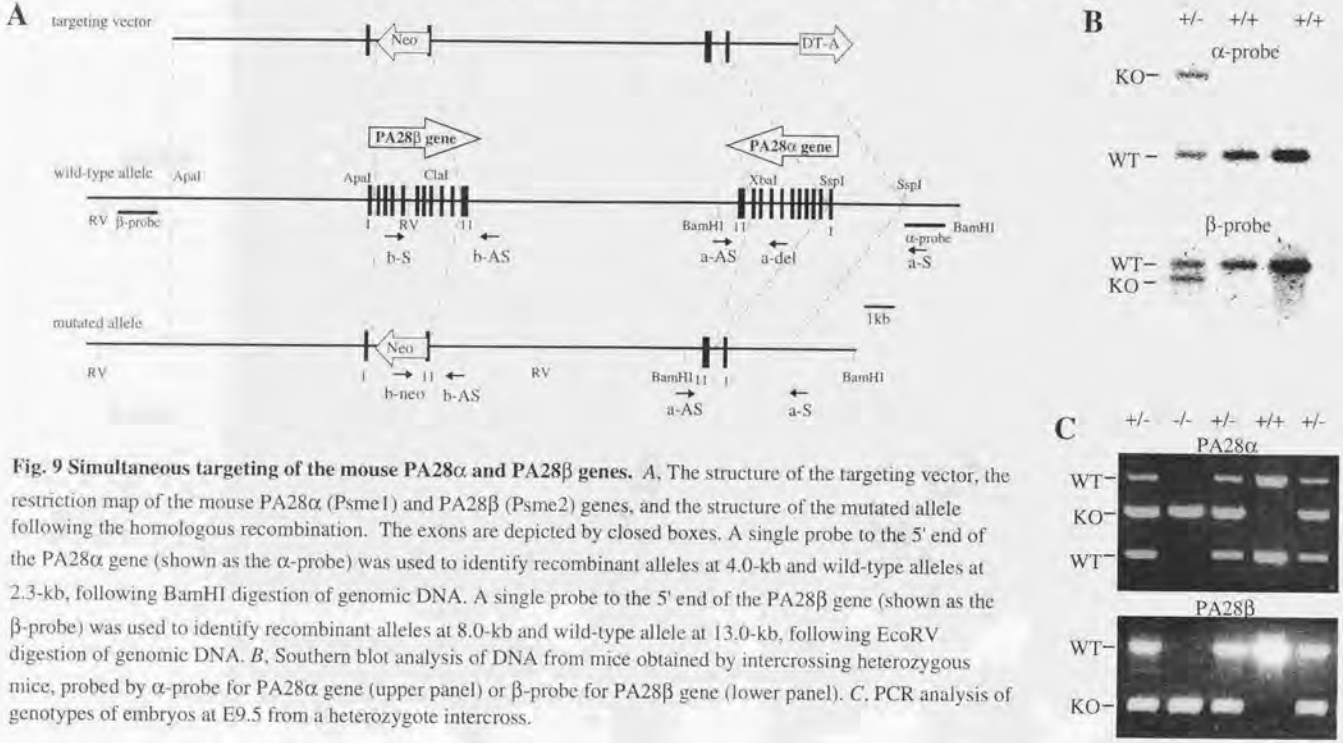


**Fig. 9 Simultaneous targeting of the mouse PA28α and PA28β genes.** *A*, The structure of the targeting vector, the restriction map of the mouse PA28α (Psme1) and PA28β (Psme2) genes, and the structure of the mutated allele following the homologous recombination. The exons are depicted by closed boxes. A single probe to the 5' end of the PA28α gene (shown as the α-probe) was used to identify recombinant alleles at 4.0-kb and wild-type alleles at 2.3-kb, following BamHI digestion of genomic DNA. A single probe to the 5' end of the PA28β gene (shown as the β-probe) was used to identify recombinant alleles at 8.0-kb and wild-type allele at 13.0-kb, following EcoRV digestion of genomic DNA. *B*, Southern blot analysis of DNA from mice obtained by intercrossing heterozygous mice, probed by α-probe for PA28α gene (upper panel) or β-probe for PA28β gene (lower panel). *C*. PCR analysis of genotypes of embryos at E9.5 from a heterozygote intercross.

wild-type

PA28α/β -/-

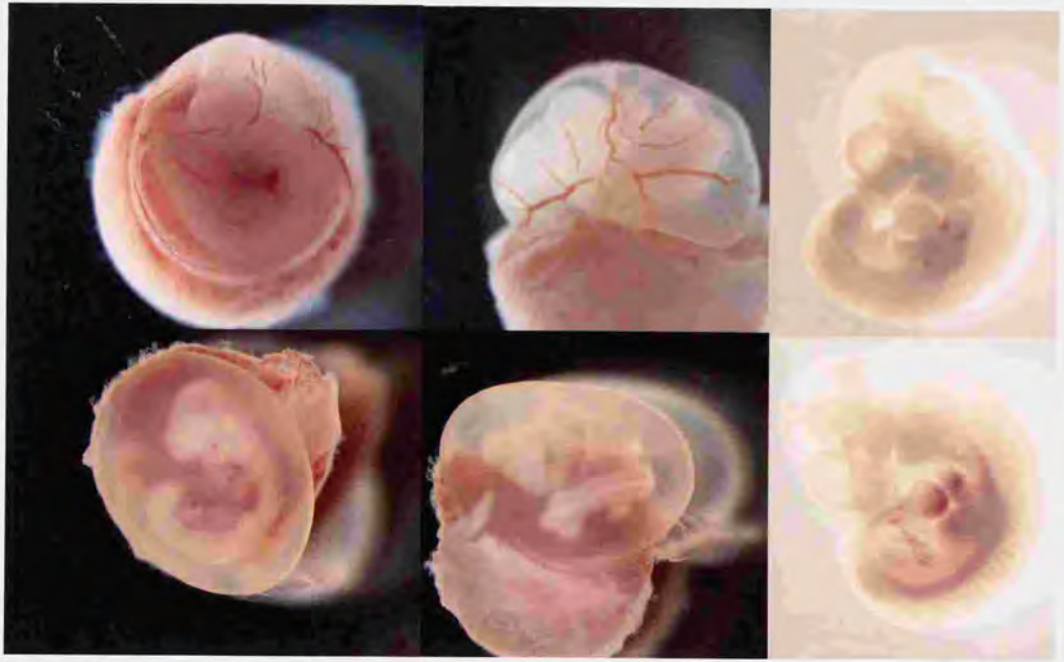

**Fig. 10 Morphology of E10.5 embryos.**
At E10.5 mutant embryos are already dead, showing pale yolk sac and arrested heart. But the size of embryos and the developmental stage are alomost the same as their littermates.

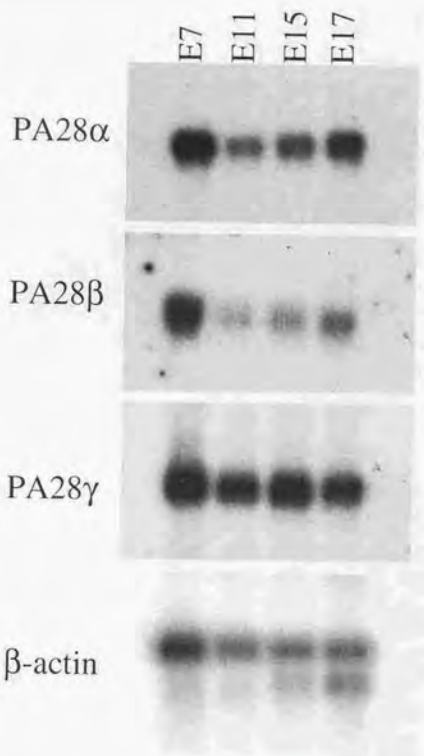


**Fig. 11 The expression levels of three PA28 genes in mouse development.** A filter blotted poly(A)$^+$ RNAs of mouse embryos at various developmental stages was probed with PA28α, PA28β, or PA28γ cDNA.

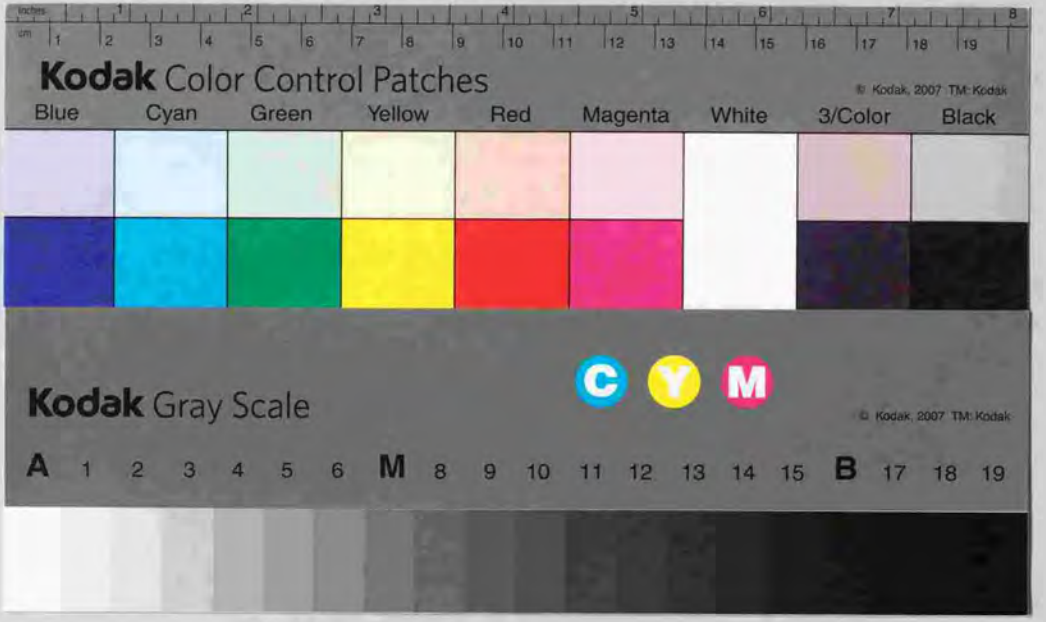
Kodak Color Control Patches
© Kodak, 2007 TM: Kodak
Blue
Cyan
Green
Yellow
Red
Magenta
White
3/Color
Black
Kodak Gray Scale
C
Y
M
© Kodak, 2007 TM: Kodak
A 1 2 3 4 5 6 M 8 9 10 11 12 13 14 15 B 17 18 19